



Structure, morphology, and optical properties of ZnO:Mg thin film prepared by sol-gel spin coating method

Budi Astuti*¹, Putut Marwoto², Azizah Zhafirah³, Nur Hamid⁴, Didik Aryanto⁵, Sugianto⁶, Sulhadi⁷, Ngurah Made Dharma Putra⁸, Fianti⁹

^{1, 2, 3, 4, 6, 7, 8, 9} Physics Department, Faculty of Mathematics and Natural Sciences, Universitas Negeri Semarang
⁵ Research Center for Physics, Indonesian Institute of Sciences, Indonesia

*Corresponding Address: b_astuti79@mail.unnes.ac.id

Article Info

Article history:

Received: January 04, 2021
 Accepted: August 26, 2021
 Published: October 30, 2021

Keywords:

Morphology properties;
 Optical Properties;
 The sol-gel spin coating method;
 Structure properties;
 ZnO: Mg thin film.

ABSTRACT

This research was conducted to analyze the Mg doping concentration effect on the structure, morphology, and optical properties of ZnO thin film prepared using the sol gel spin coating method. The Mg concentration was varied in the mole fraction of 1%, 3%, and 5%. Firstly, ZnO: Mg solution was dropped on a substrate and grown with a rotating speed of 3000 rpm and then annealed at 500 °C for 2 hours. The characterization of thin films' structure, morphology, and optical properties was done using XRD, FESEM, EDX, and UV-VIS spectrophotometer. XRD result showed a polycrystalline structure with three dominant peaks of (100), (002), and (101) plane, hexagonal wurtzite structures. Furthermore, the crystallite size was increased with the increase of Mg doping. FESEM results showed that the 5% ZnO: Mg thin film was the densest and least void from other films. In addition, the results of UV-Vis-NIR analysis showed the highest absorption value at a wavelength of 360-370 nm. The bandgap energy increased at 1% and 3% Mg doping samples but decreased by 5% Mg doping comes from the excess of oxygen in thin film with 5% Mg doping.

© 2021 Physics Education Department, UIN Raden Intan Lampung, Indonesia.

INTRODUCTION

Thin film technology has undergone many developments, both in terms of the materials used, the method of manufacture, and their application. Common Materials used in thin films preparation are InO (Kim et al., 2012), WO₃ (Dalavi et al., 2013), SnO₂ (Sharma et al., 2011), TiO₂ (Behpour et al., 2015), ZnO (Bhadane et al., 2014), ITO (Vaishnav et al., 2015) and many other materials. ITO, Indium Tin Oxide material is widely used in several fields such as the manufacture of liquid crystal displays (LCD) (Xia & Gerhardt, 2016), plasma display panels (PDPs) (Hori & Mizuno, 2012), organic light-emitting diodes (OLEDs) (Xiang et al., 2015), as well as the window layer in solar cells (Chung et al., 2012). This

is because ITO thin film has a conductivity of around $10^4 \Omega^{-1} \text{cm}^{-1}$ and a transmittance of about 85% with a bandgap of 3.70 eV (Sugianto et al., 2016). However, ITO also has weaknesses, namely Indium material, which is expensive and relatively rare (Alghamdi et al., 2014), so new material is needed to replace ITO's weakness.

Zinc oxide semiconductors (ZnO) can replace ITO because of their main advantages of being cheap and non-toxic (Li et al., 2021), wide bandgap energy of 3.37 eV (Aryanto et al., 2016), and high binding energy of 60 MeV at room temperature (Abed et al., 2020). However, ZnO thin films without doping have poor electrical characteristics, e.g., a low conductivity (Ponja et al., 2020). The deficiencies of pure

ZnO can be corrected by doping, and the doping materials are aluminum (Astuti et al., 2018), gallium (Sulhadi et al., 2015), manganese (Cao et al., 2018), and magnesium (Siregar, et al., 2020).

Magnesium (Mg) was chosen because the Mg^{2+} ion has an ionic radius of 0.65 Å, almost the same as the Zn^{2+} ionic radius of 0.74 Å. Adding Mg^{2+} in ZnO will not cause huge lattice changes in the ZnO wurtzite crystal lattice (Yuechan Li et al., 2021). Merging MgO with ZnO can increase the bandgap energy from 3.32 – 3.51 eV concerning increases in Mg concentration (Kasi & Seo, 2019). According to Zhang et al. (2011), if Mg-doped ZnO, it was not only the band gap value that increased from undoped ZnO, but the conductivity value also increased. In addition, Kulandaisamy et al. (2016) also reported that the increasing Mg concentration would decrease the resistivity of ZnO thin films.

There are several methods to grow thin films of ZnO doping Mg, i.e., molecular beam epitaxy (Pham et al., 2021), plasma-enhanced chemical vapor deposition (Hacini et al., 2021), pulsed-laser deposition (Haider et al., 2021), RF magnetron sputtering (Lin et al., 2021), thermal evaporation (Lad et al., 2021), sol-gel (Baig et al., 2021), and spin coating (Siregar et al., 2020). The sol-gel spin coating method was conducted in this research to grow the thin films. Its method has several advantages in controlling film composition, high homogeneity, adjustable thickness, coating capability over a large area, and low production costs. However, several factors need to be considered concerning the growth of ZnO thin films,

i.e., solution concentration, substrate handling, annealing temperature, solvent, and film thickness (Gahtar et al., 2014). The effect of solution concentration has not been much developed so far. This research was focused on the analysis of the Mg concentration effect on the crystal structure, morphology, and optical properties of the ZnO thin films. According to these properties, the ZnO thin films doped Mg are suitable for solar cell application window layer material.

METHODS

The thin film was grown on a corning glass by using the sol-gel spin coating method. Mg was doped into ZnO sol-gel solution via zinc acetate dehydrate as the main precursor, magnesium tetrahydrate as a doping agent, isopropanol as a solvent, and ethanolamine as a stabilizer. Solutions were prepared with varied Mg concentration, i.e. 0%, 1%, 3%, and 5%. The precursor and dopant solution were prepared at 0.5 M in 20 mL of isopropanol and stirred with a magnetic stirring for 15 mins at 60 °C. The final solution was a highly homogeneous and transparent blue color solution. The solution was aged for 24 hours at room temperature to avoid any residue rising. After that, the gel was dropped on the corning glass substrate and spun at 300 rpm for 15 seconds. The schematic of the experimental procedure is shown in Figure 1. The thin films were characterized by using X-Ray Diffraction (XRD), Scanning Electron Microscopy (SEM), Energy Dispersive X-Ray (EDX), and UV-Vis-NIR spectrophotometer.

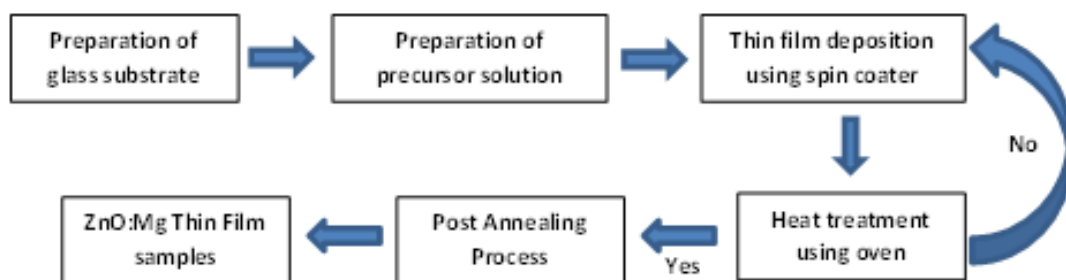


Figure 1. The Schematic of the ZnO: Mg Thin Film Grown by Using Sol-Gel Spin Coating Method

RESULT AND DISCUSSION

Structure

The XRD patterns of the un-doped and doped ZnO are shown in Figure 2. XRD patterns were suitable to ICDD (International Center for Diffraction Data) date base No. 01-078-3315. All samples of ZnO have a polycrystalline structure with diffraction peaks at 2Theta of 31.74, 34.53, 36.21, 47.53, 56.55, 62.85, and 67.92° sequentially with (100), (002), (101), (102), (110), (103), and (112) planes. Thus, the crystal structure was hexagonal wurtzite (Abed et al., 2015). Figure 2 showed three dominant peaks, i.e., plane (100), (002), and (101). Since peaks of (002) and (101) were too close, then the preferred orientation was determined by using its texture coefficient (TC) calculation as follow (Romero et al., 2006; Pandey et al., 2021):

$$TC = \left(\frac{I_{(hkl)}/I_{r(hkl)}}{[1/n \sum I_{(hkl)}/I_{r(hkl)}]} \right), \quad (1)$$

Where $I(hkl)$ was the XRD intensity of the thin film, n was several reflections observed in the XRD pattern, and $I_r(hkl)$ was the reference intensity of the ICDD database.

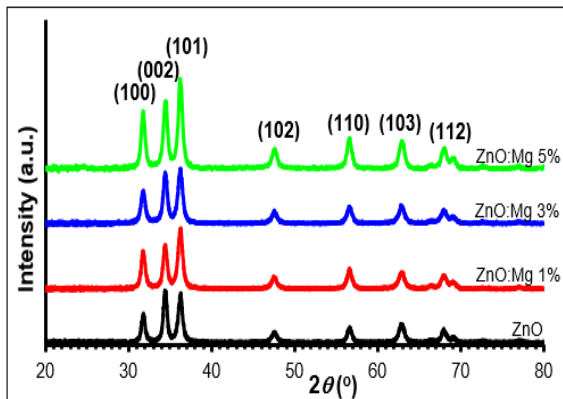


Figure 2. XRD Diffractogram of ZnO: Mg Thin Film with Different Concentration of Mg

TC value indicated the maximum preferential orientation of the films along the diffraction plane. A preferential crystal field was identified if TC value > 1. The texture coefficient values of the three dominant orientation planes are shown in Table 1.

Table 1. Texture Coefficient of Mg-doped ZnO Thin Film

Mg Concentration	Plane Orientation		
	100	002	101
ZnO	0.76	1.72	0.71
ZnO: Mg 1%	0.93	1.39	0.83
ZnO: Mg 3%	0.81	1.61	0.75
ZnO:Mg 5%	0.92	1.41	0.81

Table 1 showed that plane (002) had a TC value > 1 at all thin films. This indicates the preferential orientation of the Mg doped ZnO thin film was (002) plane along the c -axis.

FWHM value was obtained from the half-width value of the diffraction peak. FWHM was converted into radians by multiplying $\pi/180$. The crystal size D was calculated using the Scherrer equation (Hacini et al., 2021),

$$D = \frac{0,9\lambda}{\beta \cos \theta}, \quad (2)$$

Where β was the FWHM of the highest peak (hkl), λ was the X-ray wavelength (1.542 Å), and θ was the diffraction 2Theta of Bragg. The lattice parameter c was calculated by using equation 3 (Astuti et al., 2020):

$$c = \frac{\lambda}{2 \sin \theta} l, \quad (3)$$

Where λ was the X-ray wavelength and hkl was the Miller index. Lattice strain (ϵ) was calculated by using the following equation (Idris & Subramani., 2020),

$$\epsilon = \frac{\beta}{4 \tan \theta}, \quad (4)$$

The strain affected the length of the dislocation line per unit crystal volume (dislocation density). The relationship between strain and dislocation density (ρ) can be expressed by,

$$\rho = \left[\frac{\sqrt{12}\epsilon}{d} \right] \quad (5)$$

where d was the d -spacing of different crystal planes (hkl) for the hexagonal structure determined using the equation 6,

$$\frac{1}{d^2} = \frac{4(h^2+hk+l^2)}{3a^2} + \left(\frac{l^2}{c^2} \right). \quad (6)$$

The FWHM value, crystal size, lattice parameter c , strain, and dislocation density are shown in Table 2.

Table 2 showed that the FWHM was inversely proportional to the crystal size, where the smaller FWHM indicated the larger crystal size, corresponding to the Scherrer equation. The c lattice parameter of

Mg-doped ZnO was greater than the undoped ZnO, 5.207 Å, caused by a pressure leading to a positive strain at ZnO thin film. The c lattice constant decreased with the Mg concentration increasing because the addition of Mg doping into ZnO contributed to the pressure reduction in the film.

Tabel 1. Parameter of FWHM, Crystallite Size, Lattice Constant of (002) Plane

Mg Concentration	h k l	FWHM	D (nm)	Lattice Constant	ϵ (%)	ρ (line/nm ²)
0%	002	0.503	16.647	5.2160	0.0070	0.0056
1%	002	0.564	14.863	5.2165	0.0078	0.0070
3%	002	0.561	14.885	5.2160	0.0077	0.0069
5%	002	0.555	15.135	5.2101	0.0077	0.0068

The doped ZnO crystal size decreased then increased with the increasing of the Mg concentration due to the incorporation of Mg atoms resulting in ZnO lattice strain. These larger crystallite sizes led to better crystallinity because low grain boundaries resulted in fewer defects in the film (Hashim et al., 2017). The film strain and dislocation density were quite low. The low value of strain and dislocation density indicated a good crystal quality. Dislocations indicated an imbalance in the orientation of the adjacent parts in the growing crystal rising vacancy or interstitial atoms. This triggered a defect crystallization.

The lattice strain and the dislocation density affected the crystal size. The crystal size depended on the atomic radius in a crystal. The size of the ionic radius Mg^{2+} (0.65 Å) was in the same order as the ionic radius of Zn^{2+} (0.74 Å). Such large differences in ionic radii resulted in interstitial crystal defects or insertions. This was consistent with the resulting XRD pattern, where all the resulting diffraction peaks were diffraction peaks of the ZnO thin film. The addition of Mg concentration to ZnO thin films only affected the quality of the crystals to be better but did not change the structure of the ZnO thin films (Fang et al., 2014).

Morphology

FESEM images of Mg-doped ZnO with 0%, 1%, 3%, and 5% varied concentration are shown in Figure 3. The images showed inhomogeneous nano-sized particles of the films. At 0%, 1%, and 3% Mg-doped films, the film's surface morphology appeared uniform, and there were voids between the grains. Meanwhile, in 5% Mg-doped film, the granular appeared the densest or least void. This was because the doping material of Mg with a higher concentration can affect the growth of ZnO, which results in small granularity. An increase in the nucleation number led to the formation of small grains during the incorporation of dopants into the ZnO material.

The EDX results of ZnO: Mg, Table 3, revealed that the sol-gel technique was a good method to ensure no contaminant elements in preparing the thin films where only Zn, O, and Mg elements were identified. The results of this EDX analysis corresponded to XRD analysis, where the crystalline structure only belongs to ZnO peaks and no diffraction peaks from Mg. It figured out the success of Mg incorporation into the ZnO structure. This showed that Mg doping did not change the structure of the ZnO thin film structure but only the insertion of Mg elements in the ZnO thin film structure. This result was similar to research conducted by Lekoui et al. (2021).

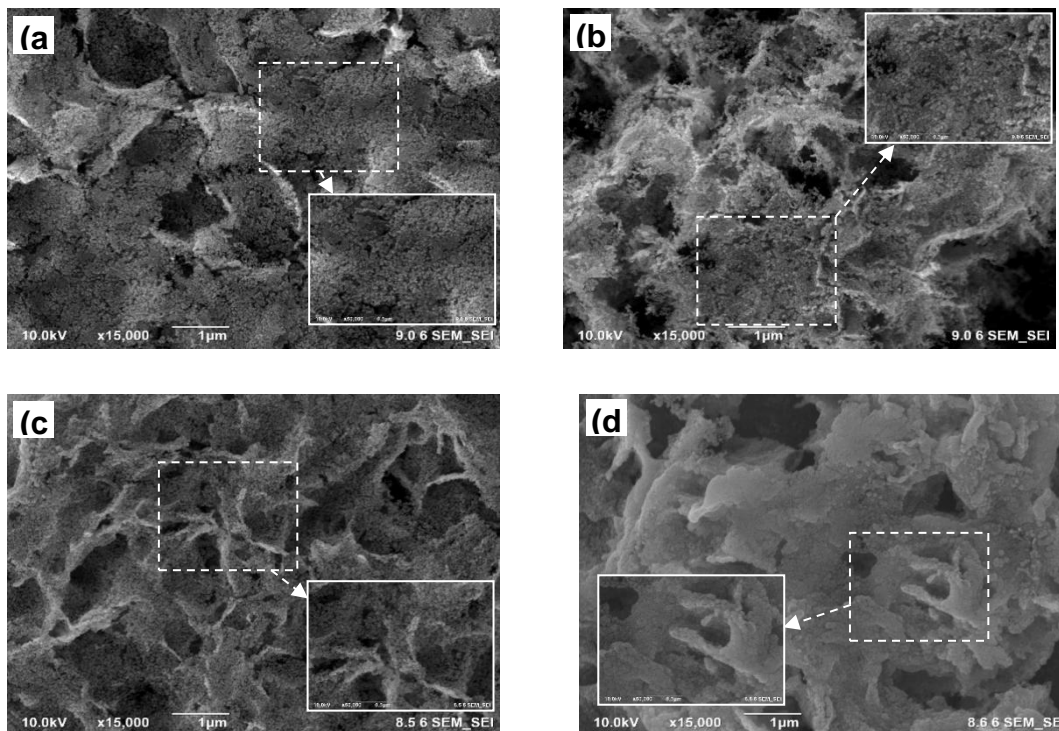


Figure 3. FESEM Images of Mg Doped ZnO Thin Film with (a) 0%, (b) 1%, (c) 3%, and (d) 5% Varied Concentration

Table 3. Ratio compositional of Mg doped ZnO thin film

	Zn (%)	O (%)	Mg (%)
ZnO	50.1	49.9	-
ZnO: Mg 1 %	49.9	49.2	0.9
ZnO: Mg 3 %	47.3	50.2	2.5
ZnO: Mg 5 %	45.1	51.1	3.8

The EDX analysis showed that the percentage of the Zn composition decreased

with the increase of the Mg element in each sample. In contrast, the O content increased with the addition of the Mg element in the thin film, following the empirical calculations in the preparation process.

Optical Properties

The absorption value of the un-doped and doped ZnO thin films are shown in Figure 4.

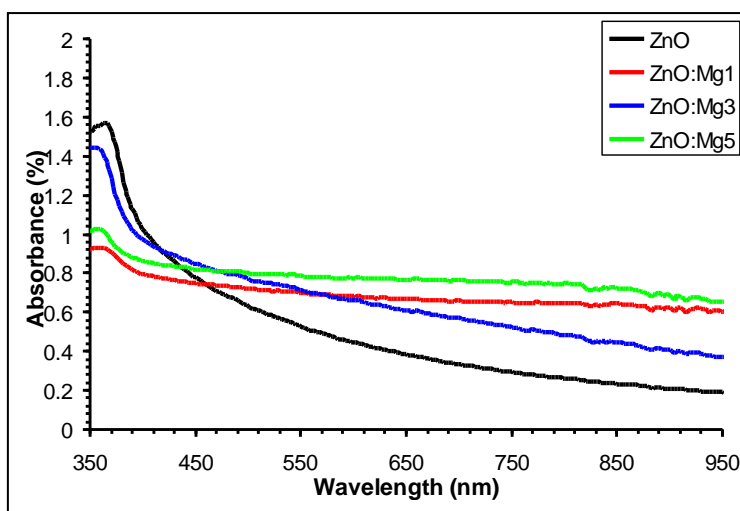


Figure 4. UV-VIS Spectra of ZnO Doping Mg Thin Film with Different Mg Concentration

In Figure 4, it can be seen that the highest absorption value on ZnO thin films was in the wavelength range of 360-370 nm, i.e., ZnO thin film can absorb in the area of the ultraviolet region (Mia et al., 2017; Siregar et al., 2020). Based on this absorption region, then can be calculated the bandgap energy by the Touch plot method using the equation:

$$(\alpha h\nu)^{1/2} = A(H\nu - E_g) \quad (7)$$

Where α was the absorption coefficient, h was Plank's constant, ν was the frequency of light radiation, E_g was the bandgap energy, and the order was $1/2$ for the allowed direct transition (Pradeev raj et al., 2018). Then a graph was plotted $(\alpha h\nu)^2$ on the y-axis and $h\nu$ on the x-axis. The plot results are shown in Figure 5.

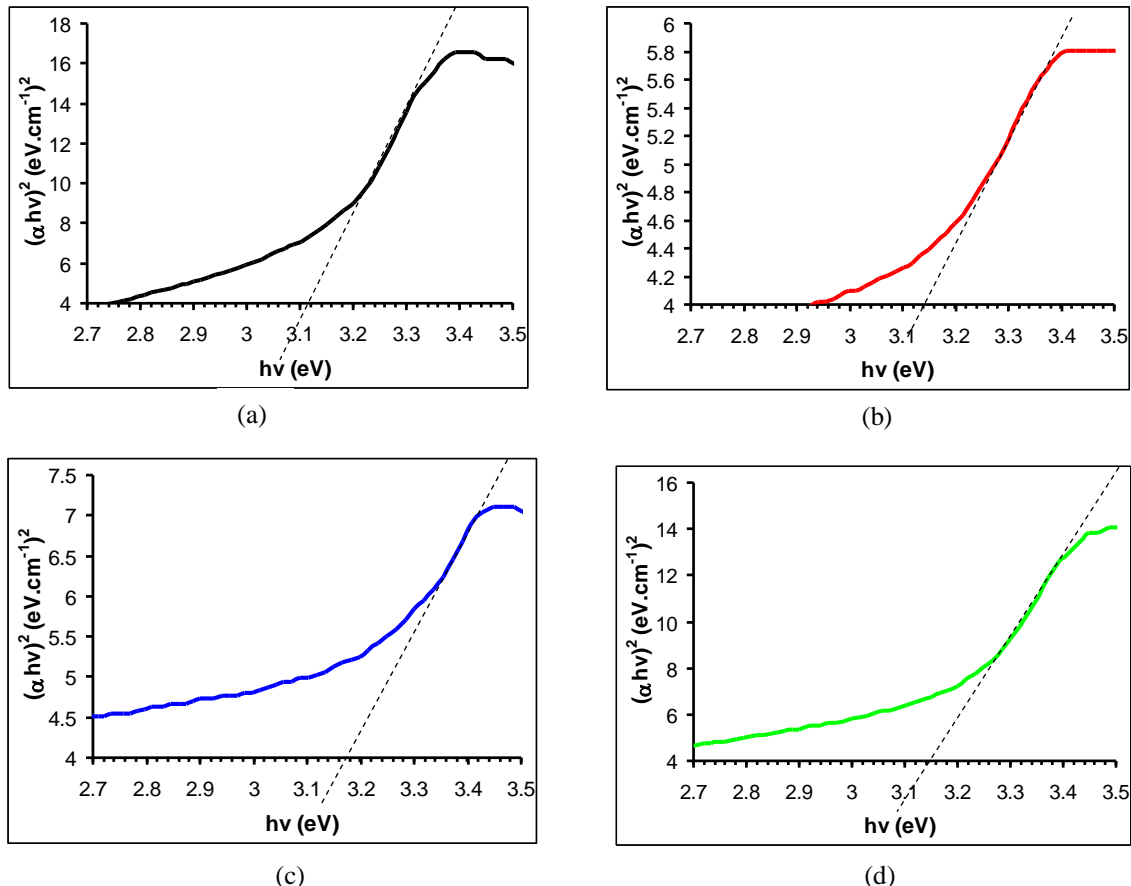


Figure 5. Band Gap Energy of Mg Doped ZnO (a) 0%, (b) 1%, (c) 3%, and (d) 5% Varied Mg Concentration

Bandgap energy of ZnO thin films increased in 1% and 3% Mg doping but decreased in 5% Mg doping. Bandgap energy of Mg doped ZnO thin film can be seen in Table 4. The bandgap energy increased with the Mg doping concentration (Thonglem et al., 2016), and the edge of the band shifted to the lower wavelength side (higher energy) or the so-called blue shift as known as the Burstein-Moss effect (Siregar et al., 2021).

Table 4. Band Gap Energy of Mg Doped ZnO

Mg Concentration (%)	Band Gap Energy (Ev)
0	3.11
1	3.14
3	3.17
5	3.14

This shift can be attributed to an increase in the concentration of charge carriers in the conduction band due to absorption. As the doping increases, the state close to the conduction band is filled, thereby shifting the

Fermi level, which causes the energy bandgap to widen (Priscilla et al., 2021).

The bandgap energy decreases in 5% Mg-doped ZnO thin film, its the increasing of doping gives more enhancement of order and the localized states. As we know, the higher localized state can affect the lower bandgap energy. Furthermore, the increase of Mg 5% on ZnO thin film is likely produces crystal lattice distortion and lattice defects. The FESEM result proves that Mg 5% has a higher porosity than the other, which can also affect the bandgap energy. So, we can say the 3% Mg concentration doped ZnO thin film is optimum concentration can be used. This result is similar to Haidar et al. (2020), which studied the effect of Mg concentration doped ZnO thin films with variations of 1%, 3%, and 5%, but used a different method pulsed laser deposition.

The bandgap increases and Mg concentration also increases, indicating that the ZnO: Mg thin film was a compatible material for optoelectronic device application (Huang et al., 2012).

The morphologies and optical properties correspond those voids between the grains formed at the thin film with Mg-doped 0%, 1%, and 3% let the light pass easily due to the cavity or more light transmitted through the ZnO thin films. This was following the requirements in window layers preparation which requires a material with a large bandgap and allows large light-transmitting.

CONCLUSION

Thin films of ZnO: Mg with various concentrations of Mg were deposited using the sol-gel spin coating method and have been successfully grown. The thin film Mg-doped ZnO has a hexagonal wurtzite crystal structure with a dominant peak in the orientation plane (100), (002), and (101) and has a preferential plane along the c-axis. The crystal size increased with increasing of Mg concentration. Moreover, a thin film with Mg doping of 0%, 1%, and 3% had a uniform film surface morphology with cavities between the grains, while the granules were

denser in the film with 5% Mg doping. The percentage of the Zn composition decreased with the addition of Mg in each sample, showing that Mg doping has combined with ZnO. The highest absorption occurred at a wavelength range of 360-370 nm. In addition, the bandgap value in the ZnO thin film increased in Mg doping by 1% and 3% but decreased in Mg 5% doping which was assumed because of the oxygen excess in 5% Mg-doped film. The bandgap value was in the range of 3.11-3.17 eV. The bandgap value was suitable for optoelectronic field applications. The next study was needed to measure the film's thickness and the electrical properties to get complete information of the Mg-doped ZnO thin film as window layer material on the solar cell application.

REFERENCES

- Abed, C., Bouzidi, C., Elhouichet, H., Gelloz, B., & Ferid., M. (2015). Mg doping induced high structural quality of Sol-Gel ZnO nanocrystals: Application in photocatalysis. *Applied Surface Science*, 349, 855-863.
- Abed C., Fernandes S., Aouida S., Elhouichet H., Priego F., Castro Y., Gomes-Mancebo M.M., & Munuera G. (2020). Processing and study of optical and electrical properties of (Mg, Al) co-doped ZnO thin films prepared by RF magnetron sputtering for photovoltaic application. *Materials*. 13(9), 1-12
- Al-ghamdi, A. A., Al-hartomy, O. A., Okr, M. El, Nawar, A. M., El-gazzar, S., El-tantawy, F., & Yakuphanoglu, F. (2014). Semiconducting properties of Al doped ZnO thin films. *Spectrochimica Acta Part A : Molecular and Biomolecular Spectroscopy*. 131, 512-517.
- Aryanto, D., Marwoto, P., Sudiro, T., Birowosuto, M. D., Sugianto, & Sulhadi. (2016). Structure evolution of zinc oxide thin films deposited by unbalance DC magnetron sputtering. *AIP Conference Proceedings*, 1729, 1-

- 6.
- Astuti, B., Sugianto, Mahmudah, S. N., Zannah, R., Putra, N. M. D., Marwoto, P., Aryanto, D., & Wibowo, E. (2018). Structural and morphological study on ZnO:Al thin films grown using DC magnetron sputtering. *Journal of Physics: Conference Series*, 983(1), 1-6.
- Astuti, B., Zhafirah, A., Carieta, V. A., Hamid, N., Marwoto, P., Sugianto, Nurbaiti, U., Ratnasari, F. D., Putra, N. M. D., & Ariyanto, D. (2020). X-ray diffraction studies of ZnO: Cu thin films prepared using sol-gel method. *Journal of Physics: Conference Series*, 1567(1), 1-6.
- Baig F., Asif A. Ashraf M.W., & Fahad HM. (2021). Tailoring of optical, hydrophobic and anti ising properties of Ca, Mg codoped ZnO thin films via sol gel method. *Journal of Sol-Gel Science and Technology*. 97(3), 706 -720.
- Behpour, M., Mehrzad, M., & Hosseinpour-Mashkani, S. (2015). TiO₂ thin film: Preparation, characterization, and its photocatalytic degradation of basic yellow 28 Dye. *Journal of Nanostructures*, 5(2), 183–87.
- Bhadane, H., Samuel, E., & Gautam, D. K. (2014). Influence of post annealing on sol-gel deposited ZnO thin films. *Surface Review and Letters*, 21(4), 1–6.
- Chung, C. H., Song, T. Bin, Bob, B., Zhu, R., Duan, H. S., & Yang, Y. (2012). Silver nanowire composite window layers for fully solution-deposited thin-film photovoltaic devices. *Advanced Materials*, 24(40), 5499–5504.
- Dalavi, D., Mahavidyalay, K., Budruk, R., Devan, R. S., & Patil, R. (2013). Efficient electrochromic performance of nanoparticulate WO₃ thin films. *Journal of Materials Chemistry C*, 1(23), 3722–3728.
- Fang, D., Lin, K., Xue, T., Cui, C., Chen, X., Yao, P., & Li, H. (2014). Influence of Al doping on structural and optical properties of Mg – Al co-doped ZnO thin films prepared by sol – gel method. *Journal of Alloys and Compounds*, 589, 346–352.
- Gahtar, A., Rahal, A., Benhaoua, B., & Benramache, S. (2014). A comparative study on structural and optical properties of ZnO and Al-doped ZnO thin films obtained by ultrasonic spray method using different solvents. *Optik - International Journal for Light and Electron Optics*, 123(14), 3674-3678.
- Hacini, N., Ghamnia, M., Dhamni, M.A., Boukhachem, A., Pireaux, J.J. & Houssiau, L. (2021). Compositional, structural, morphological and optical properties of ZnO thin films prepared by PECVD technique. *Coating*. 11(202), 1-11.
- Haidar A.J., Jabbar A.A., & Ali G.A. (2021). A review of pure and undoped ZnO nanostructure production and its optical properties using pulsed laser deposition technique. *Journal of Physics: Conference Series*. 1975(1), 1-12.
- Hashim, N. H., Subramani, S., Devarajan, M., & Ibrahim, A. R. (2017). Properties of undoped ZnO and Mg doped ZnO thin films by sol-gel method for optoelectronic applications. *Journal of the Australian Ceramic Society*, 53(2), 421–31
- Hori, S., & Mizuno, K. (2012). Sheet structure, method of manufacturing sheet structure, and electronic device. *Patent Application Publication*, 10, 1-10.
- Huang, K., Tang, Z., Zhang, L., Yu, J., Lv, J., Liu, X., & Liu, F. (2012). Preparation and characterization of Mg-doped ZnO thin films by sol–gel method Kai. *Applied Surface Science Jou*, 258(8), 3710–3713.
- Idris M.S. & Subramani S. (2020). Performance analisis of MgO/ZnO multilayer thin film as heat spreader on Al substrate for high power LED thermal management applications. *Journal of materials science:Material in Electerronics*, 31, 15976-15990 <https://doi.org/10.1007/s10854-020->

- 04159-z.
- Kasi G. & Seo J. (2021). Influence of Mg doping on the structural, morphological, optical, thermal and visible light responsive antibacterial properties of ZnO nanoparticles synthesized via coprecipitation method. *Science and Engineering C*, 98, 717-725.
- Kim, J., Son, D., Kim, J., Son, D., Park, S., Kim, D., Sung, S., & Jung, E. (2012). Effects of Ti addition on sol-gel derived InO and InZnO thin film transistors. *Current Applied Physics*, 12, e24–e28.
- Kulandaisamy, A. J., Reddy, J. R., Srinivasan, P., Babu, K. J., Mani, G. K., Shankar, P., & Rayappan, J. B. B. (2016). Room temperature ammonia sensing properties of ZnO thin films grown by spray pyrolysis: Effect of Mg doping. *Journal of Alloys and Compounds*, 688, 422–29.
- Lad U.D., Kokode N.S., Deore M.B. & Tupe U.J. (2021). MgO incorporated ZnO nanostructured binary oxide thin films ethanol gas sensing. *International journal of scientific development and research*, 6(1), 135 - 142.
- Lin W.Y., Chien F.T., Chiu H.C. Sheu J.K., & Hsueh K.Po. (2021). Effect of thermal annealing on the properties of Zirconium doped Mg_xZn_{1-x}O film obtained through radio frequency magnetron sputtering. *Membrane*, 11(5), 1-8.
- Li Z., Li J., Lei J., Xiong M., Wang N., & Zhang S. (2021) First principles study of structure, electrical and optical properties of Al and Mo co-doped ZnO. *Vacuum*, 186, 1-10.
- Lekoui F., Hassani S., Ouchabani M., Akkari H. Dargham D., Filali W., & Garoudja E. (2021). Elaboration and characterization of Mg doped ZnO thin films by thermal evaporation nanelaing temperature effect. *Brazilian Journal of Physics*, 51, 544-554.
- Mia, M. N. H., Pervez, M. F., Hossain, M. K., Reefaz Rahman, M., Uddin, M. J., Al Mashud, M. A., Ghosh, H. K., & Hoq, M. (2017). Influence of Mg content on tailoring optical bandgap of Mg-doped ZnO thin film prepared by sol-gel method. *Results in Physics*, 7, 2683–2691.
- Pandey A., Dalal S., Dutta S., & Dixit A. (2021). Structural characterization of polycrystalline thin film by X-ray diffraction technique. *J. Mater Sci: Mater Electron*, 32, 1341-1368.
- Ponja S.D., Sathasivaw S., Parkin I.P. & Carmalt C.J., 2020. Highly Conductive and transparent gallium doped zinc oxide thin films via chemical vapor deposition. *Scientific report*, 10, 1-7.
- Pham A.T.T., Ngoc Vo P.T., Thi Ta H.K. Lai H.T., Tran V.C. Doan T.L.H., Duong A.T., Lee C.T., Nair P.K., Zulueta Y.A., Phan T.B., & Luu S.D.N. (2021). Improved thermoelectric power factor achieved by energy filtering in ZnO:Mg/ZnO structure. *Thin Solid films*, 721, 1-7
- Pradeev raj, K., Sadaiyandi, K., Kennedy, A., Sagadevan, S., Chowdhury, Z. Z., Johan, M. R. Bin, Aziz, F. A., Rafique, R. F., Thamiz Selvi, R., & Rathina bala, R. (2018). Influence of Mg doping on ZnO nanoparticles for enhanced photocatalytic evaluation and antibacterial analysis. *Nanoscale Research Letters*, 13(229), 1-13.
- Priscilla S.J. Daniel R., Dhakshayani Y., Caroline S.C., & Sivaji K. (2021). Effect of magnesium dopant on the structural, morphological, and electrical properties of ZnO nanoparticle by sol gel method. *Material Today: Proceeding*, 36(4), 793-796.
- Romero, R., Leinen, D., Dalchiale, E. A., Ramos-barrado, J. R., & Martín, F. (2006). The effects of zinc acetate and zinc chloride precursors on the preferred crystalline orientation of ZnO and Al-doped ZnO thin films obtained by spray pyrolysis. *Thin Solid Films*, 515(4), 1942–1949.

- Sharma, A., Tomar, M., & Gupta, V. (2011). Sensors and actuators B: Chemical SnO₂ thin film sensor with enhanced response for NO₂ gas at lower temperatures. *Sensors & Actuators: B. Chemical*, 156(2), 743–752.
- Siregar, N., Moltan & Panggabean, J. (2020). The effect magnesium (Mg) on structural and optical properties of ZnO:Mg thin film by sol gel spin coating method. *Journal of Physics: Conference Series*, 14266, 1-6.
- Siregar N., Moltan, Panggabean, J.H., Sirait M., Rajagukguk J. Gultom N.S., & Sabir F.K. (2021). Fabrication of Dye sensitized solar cell (DSSC) using Mg doped ZnO as photoanode and extract of rose myrtle (*rhodomyrtus tomentosa*) as natural dye. *International Journal of Photoenergy*, 2021, 1-7.
- Sugianto, Zannah, R., Mahmudah, S. N., Astuti, B., Putra, N. M. D., AA Wibowo, Marwoto, P., Ariyanto, D., & Wibowo, E. (2016). Pengaruh temperatur annealing pada sifat listrik film tipis zinc oksida doping aluminium oksida. *Jurnal MIPA*, 39(2), 115–122.
- Sulhadi, Marwoto, P., Sugianto, & Wibowo, E. (2015). Variasi suhu deposisi pada struktur, sifat optik dan listrik film tipis seng oksida dengan doping galium (ZnO:Ga). *Jurnal Pendidikan Fisika Indonesia*, 11(1), 93–99.
- Tonglem s., Sksri C., Pengpat K., Rujijanagul G., Eitssayeam s., Intatha U. & Tunkasiri T. (2016). Tuning the band gap of ZnO thin film by Mg doping. *Key Engineering Material*, 690, 131 - 136.
- Vaishnav, V. S., Patel, S. G., & Panchal, J. N. (2015). Sensors and actuators B: Chemical development of ITO thin film sensor for detection of benzene. *Sensors & Actuators: B. Chemical*, 206, 381–388.
- Xia, N., & Gerhardt, R. A. (2016). Fabrication and characterization of highly transparent and conductive indium tin oxide films made with different solution-based methods. *Materials Research Express*, 3(11), 1–11.
- Xiang, H.-Y., Li, Y.-Q., Zhou, L., Xie, H.-J., Li, C., Ou, Q.-D., Chen, L.-S., Lee, C.-S., Lee, S.-T., & Tang, J.-X. (2015). Outcoupling-enhanced Flexible Organic Light-Emitting diodes on ameliorated plastic substrate with. *American Chemical Society*, 9(7), 7553-7562
- Yuechan Li, Young Li & An Xie. (2021). Synthesis and optical properties of B-Mg codoped ZnO nanoparticles. *Coatings*, 11(882), 1-10.
- Zhang, L. Q., Ye, Z. Z., Huang, J. Y., Lu, B., He, H. P., Lu, J. G., Zhang, Y. Z., Jiang, J., Zhang, J., Wu, K. W., & Zhang, W. G. (2011). Fabrication and properties of p-type K doped Zn_{1-x}Mg_xO thin film. *Journal of Alloys and Compounds*, 509(27), 7405–7409.